Journal of the Physical Society of Japan
Vol. 71, No. 12, December, 2002, pp. 2843–2846

Structures and Electromagnetic Properties of New Metal-Ordered Manganites: $R\mathrm{BaMn_2O_6}$ (R = Y and Rare-Earth Elements)

Tomohiko NAKAJIMA*, Hiroshi KAGEYAMA, Hideki YOSHIZAWA[1] and Yutaka UEDA

Materials Design and Characterization Laboratory,
[1]*Neutron Scattering Laboratory, Institute for Solid State Physics, University of Tokyo,*
5-1-5 Kashiwanoha, Kashiwa, Chiba 277-8581

(Received July 11, 2002)

New metal-ordered manganites $R\mathrm{BaMn_2O_6}$ can be classified into three groups based on the structural and electromagnetic properties measured. The first group (R = Tb, Dy and Ho) shows three successive phase transitions, namely, structural, charge/orbital order (CO) and antiferromagnetic order (AF) transitions on cooling, as observed in $\mathrm{YBaMn_2O_6}$. The second group (R = Sm, Eu and Gd) exhibits a CO transition, followed by an AF transition. The third group (R = La, Pr and Nd) exhibits a metallic ferromagnetic transition, followed by an A-type AF transition in $\mathrm{PrBaMn_2O_6}$ and $\mathrm{NdBaMn_2O_6}$. Compared with metal-disordered $(R^{3+}_{0.5}A^{2+}_{0.5})\mathrm{MnO_3}$, $R\mathrm{BaMn_2O_6}$ has two remarkable features: (1) the high CO transition temperature (T_{CO}) above 340 K and (2) the presence of a structural transition above T_{CO} in the first group. These are closely related to the structural feature that the $\mathrm{MnO_2}$ sub-lattice is sandwiched by two types of rock-salt layers, RO and BaO, with different lattice sizes.

KEYWORDS: new metal-ordered manganites $R\mathrm{BaMn_2O_6}$, structural and electromagnetic properties, structural transition, charge/orbital order, magnetic transition, phase diagram
DOI: 10.1143/JPSJ.71.2843

The magnetic and electrical properties of perovskite manganites with the general formula $(R^{3+}_{1-x}A^{2+}_{x})\mathrm{MnO_3}$ (R = rare earth elements and A = alkaline earth elements) have been extensively investigated for the last decade.[1)] Among the interesting features are the so-called colossal magnetoresistance (CMR) and metal–insulator (MI) transition accompanied by the charge and orbital order (CO). It is now widely accepted that these interesting phenomena are caused by the strong correlation/competition of multi-degrees of freedom, that is, spin, charge, orbital and lattice.

The structure of perovskite $R\mathrm{MnO_3}$ consists of a $\mathrm{MnO_2}$ square sublattice and a RO rock-salt sublattice. The mismatch between the larger $\mathrm{MnO_2}$ and smaller RO sublattices is relaxed by tilting $\mathrm{MnO_6}$ octahedra, leading to the lattice distortion from a cubic structure to, mostly, an orthorhombic $\mathrm{GdFeO_3}$-type structure. In this lattice distortion, the bond angle $\angle$Mn–O–Mn deviates from 180°, resulting in a significant change in the effective one-electron bandwidth (W) or equivalent e_g-electron transfer interaction (t). In the substitution system of $(R^{3+}_{1-x}A^{2+}_{x})\mathrm{MnO_3}$ with a fixed x and a random distribution of R^{3+} and A^{2+}, the structural and electromagnetic properties have been explained well by the degree of mismatch, that is, the tolerance factor $f = (\langle r_{\mathrm{A}}\rangle + r_{\mathrm{O}})/[\sqrt{2}(r_{\mathrm{Mn}} + r_{\mathrm{O}})]$, where $\langle r_{\mathrm{A}}\rangle$, r_{Mn} and r_{O} are (averaged) ionic radii for the respective elements, because W or t is changed by varying f. Figure 1 shows the generalized phase diagram for $(R^{3+}_{0.5}A^{2+}_{0.5})\mathrm{MnO_3}$,[1)] where the ferromagnetic metal (FM) generated by the double-exchange (DE) interaction is dominant near $f = 1$ (maximal W or t), while the CE-type CO insulator (COI(CE)) is most stabilized in the lower f region ($f < 0.975$). In the middle region ($f \sim 0.975$), the competition between the ferromagnetic DE and antiferromagnetic CO interactions results in various phenomena including CMR.

Recently, it has been argued how the A-site randomness affects the physical properties of $(R^{3+}_{1-x}A^{2+}_{x})\mathrm{MnO_3}$. The phenomena such as the coexistence of FM and CO and the electronic phase separation[2)] may be induced by the A-site randomness. Unfortunately, almost all the works devoted to a series of perovskite manganites so far are on disordered manganites with R^{3+} and A^{2+} ions being randomly distributed. This means that, whenever x is finite, there inevitably exists a disorder in the lattice. Since the physical properties of the perovskite manganite are quite sensitive to even a tiny change in lattice distortion, it is important to employ a compound without A-site disorder in order to clarify the effect of A-site randomness.

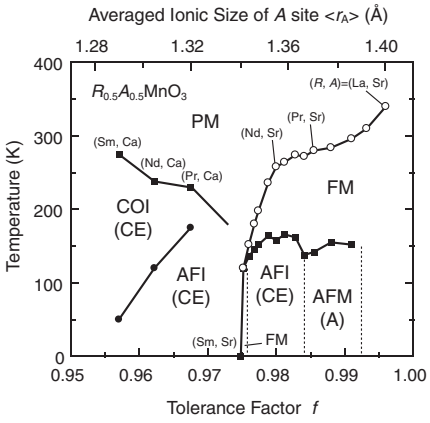

Fig. 1. Generalized phase diagram for $(R^{3+}_{0.5}A^{2+}_{0.5})\mathrm{MnO_3}$ (ref. 1). FM: ferromagnetic metal, AFM(A): A-type antiferromagnetic metal, COI(CE): CE-type charge/orbital-ordered insulator, AFI(CE): antiferromagnetic CE-type charge/orbital-ordered insulator, PM(or PI): paramagnetic metal (or paramagnetic insulator) phases.

Very recently, we have successfully synthesized a metal-ordered manganite $\mathrm{YBaMn_2O_6}$ with successive stacking of YO–$\mathrm{MnO_2}$–BaO–$\mathrm{MnO_2}$–YO [see Fig. 2(a)] and observed three successive phase transitions, namely, structural transi-

*E-mail: t-nakaji@issp.u-tokyo.ac.jp

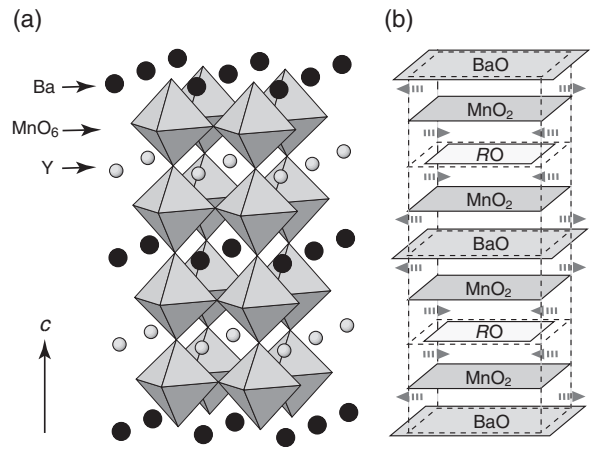

Fig. 2. Crystal structure of $YBaMn_2O_6$ (a) and a schematic illustration of structural concept for $RBaMn_2O_6$ (b). The MnO_2 square lattice is sandwiched by two types of the rock-salt layers, RO and BaO, with different lattice sizes.

tion without any charge and magnetic order at $T_t = 520$ K, CO transition (MI transition) at $T_{CO} = 480$ K and antiferromagnetic order (AF) transition at $T_N = 195$ K.[3–5] The observed $T_{CO} = 480$ K is, to the best of our knowledge, the highest among the perovskite manganites. Across the phase transition at $T_t = 520$ K, associated with the structural change from pseudo-orthorhombic (triclinic) to pseudo-tetragonal (monoclinic) on cooling, the resistivity (ρ) shows slight change and the magnetic susceptibility (χ) exhibits a large reduction. Furthermore, the magnetic interaction in the paramagnetic metal (PM) phase seems to be changed from ferromagnetic above T_t to antiferromagnetic below T_t. Such transition was first observed in perovskite manganites. The expectation that such novel transition could be closely related to the metal-ordered structure led us to study the metal-ordered perovskite manganites $RBaMn_2O_6$. In this paper, we report the structures and physical properties of the new $RBaMn_2O_6$. We summarize the results in a phase diagram and compare the diagram with Fig. 1.

Powder samples were prepared by a solid-state reaction of R_2O_3, $BaCO_3$ and MnO_2 similar to that used for $YBaMn_2O_6$.[3] No perovskite-type compound was produced for Ce, Yb and Lu. Since Er and Tm compounds included a significant amount of impurities, we excluded them from the present study.

The crystal structure was determined at 300–573 K by powder X-ray diffraction using CuKα radiation. The superstructure associated with the CO was investigated by transmission electron microscopy (TEM). The magnetic properties were studied using a SQUID magnetometer in the temperature range of $T = 5$–700 K under a magnetic field of 0.1 T. The electric resistivity of a sintered pellet was measured at $T = 100$–620 K by a conventional four-probe technique.

The X-ray diffraction patterns of all compounds clearly show the (0,0,1/2) reflection indexed with the simple cubic perovskite structure, which indicates the same metal-ordered structure as that of $YBaMn_2O_6$. The crystal structure at room temperature is a tetragonal $a_p \times a_p \times 2c_p$ one with no tilt of MnO_6 octahedra in La, Pr and Nd compounds, while in the compounds with $R = \text{Sm} \sim \text{Ho}$, it has a larger cell of $\sqrt{2}a_p \times \sqrt{2}b_p \times 2c_p$ with a tilt of MnO_6 octahedra, where a_p, b_p and c_p denote the primitive cell for the simple cubic perovskite. The $\sqrt{2}a_p \times \sqrt{2}b_p \times 2c_p$ unit cells for $R = $ Sm, Eu and Gd are tetragonal ($a_p = b_p$) but those for $R = $ Tb, Dy and Ho are distorted to monoclinic as observed in $YBaMn_2O_6$.[4,5] TEM at room temperature has revealed the in-plane superstructure of $2\sqrt{2}a_p \times \sqrt{2}b_p$ characteristic of the CE-type CO in the compounds with $R = \text{Sm} \sim \text{Ho}$, as observed in $YBaMn_2O_6$,[4] while no superstructure has been observed in the compounds with $R = $ La, Pr and Nd. In addition to such superstructure within the a–b plane, TEM has revealed a 4-fold periodicity along the c-axis, suggesting a new stacking pattern.[4]

$RBaMn_2O_6$ can be classified into three groups based on the obtained structural and electromagnetic properties. Figure 3 shows the temperature dependence of χ and ρ for

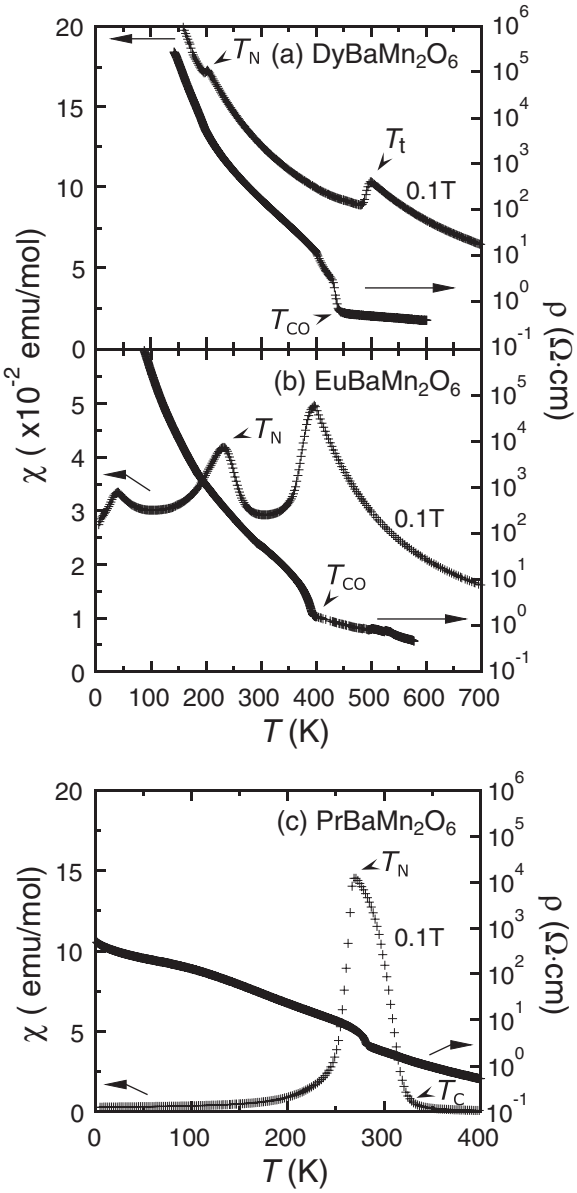

Fig. 3. Temperature dependence of resistivity (ρ) and magnetic susceptibility (χ) for (a) $DyBaMn_2O_6$, (b) $EuBaMn_2O_6$ and (c) $PrBaMn_2O_6$. $DyBaMn_2O_6$ shows a structural transition without any charge and magnetic order at T_t (see text). T_{CO}, T_N, and T_C represent the charge/orbital-ordered, antiferromagnetic and ferromagnetic transition temperatures, respectively.

(a) $DyBaMn_2O_6$, (b) $EuBaMn_2O_6$ and (c) $PrBaMn_2O_6$ as typical examples of each group. The first group includes compounds with $R^{3+} = Tb^{3+}$, Dy^{3+} and Ho^{3+} whose ionic radii are close to Y^{3+}. As can be seen in Fig. 3(a), these compounds show distinct three transitions, namely, structural (triclinic to monoclinic) transition at T_t, CO (MI) transition at T_{CO} and AF transition at T_N on cooling, as observed in $YBaMn_2O_6$.[3–5] The change of magnetic interaction from ferromagnetic above T_t to antiferromagnetic below T_t is not very evident in these compounds as in $YBaMn_2O_6$,[3] because of the significant contribution of magnetic rare-earth ions to the total χ. However the reduction of χ at T_t commonly observed in this series can be ascribed to a change in Weiss temperature, namely, a change of magnetic interaction, between the PM phases above and below T_t. The second group consists of $RBaMn_2O_6$ with $R^{3+} = Sm^{3+}$, Eu^{3+} and Gd^{3+}. The compounds exhibit a CO (MI) transition as determined by ρ [see Fig. 3(b)] and TEM (the in-plane superstructure of $2\sqrt{2}a_p \times \sqrt{2}b_p$) measurements. The structural transition as observed at T_t in the first group is absent in the second group. As shown in Fig. 3(b), the χ–T curve of $EuBaMn_2O_6$ has two anomalies at around 240 K and 40 K in addition to the reduction of χ at T_{CO}. The reduction of χ at T_{CO} is mainly due to the change of magnetic interaction from ferromagnetic to antiferromagnetic, because the ferromagntic spin-spin correlation due to DE interaction is dominant in the PM phase above T_{CO}, while the paramagnetic CO phase below T_{CO} has an antiferromagnetic one. Since the CE-type COI(CE) phase is known to order antiferromagnetically (see Fig. 1), it would be natural to ascribe one of the two anomalies of χ to AF. Actually the neutron magnetic diffraction performed in $YBaMn_2O_6$,[4] $HoBaMn_2O_6$ and $TbBaMn_2O_6$ has revealed that the anomaly of χ at around 200 K corresponds to AF. However it is difficult to perform the neutron diffraction in the second group, because of the strong absorption of neutron by rare-earth atoms. Fortunately, all of the compounds with $R = Sm \sim Ho$ and Y have similar anomalies of χ at around 200 K and 50 K below T_{CO}. Assuming that the spin-spin correlation in the CE-type COI(CE) phase is not significantly changed in $RBaMn_2O_6$, we regard the anomaly at around 200 K as T_N. No significant change was observed around 50 K in the neutron diffraction pattern. Any slight change in spin structure may occur at around 50 K. The third group $RBaMn_2O_6$ with $R^{3+} = La^{3+}$, Pr^{3+} and Nd^{3+} exhibits a FM transition at T_C, which is evidenced by the rapid increase of χ, as shown in Fig. 3(c). The observed $T_C = 335$ K for $LaBaMn_2O_6$ agrees well with the previous report.[6] In $PrBaMn_2O_6$, the FM transition is followed by some transition accompanied by the sharp reduction of χ, as shown in Fig. 3(c). The preliminary neutron magnetic diffraction has revealed a transition to *A*-type antiferromagnetic metal [AFM(A)] from FM in $PrBaMn_2O_6$ and $NdBaMn_2O_6$, which is consistent with the relatively low ρ below T_N compared with that in the COI(CE) state of $EuBaMn_2O_6$ or $DyBaMn_2O_6$ (see Fig. 3). A similar *A*-type AFM(A) was previously reported in metal-disordered $Pr_{0.5}Sr_{0.5}MnO_3$ with $f \sim 0.985$ (see Fig. 1).[7] A detailed report of the neutron diffraction study is now in preparation. A semiconductive behavior in the PM state of $PrBaMn_2O_6$ is due to loosely sintered samples. The measurements of ρ and χ in the last group were not carried out above 400 K because no transition above this temperature was detected by differential scanning calorimetry.

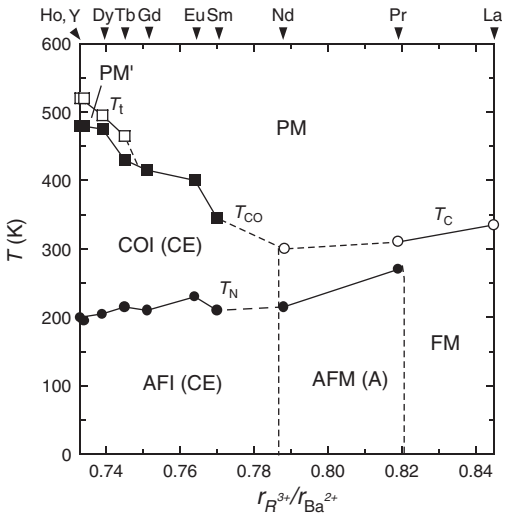

Fig. 4. Phase diagram for $RBaMn_2O_6$. The notations for each phase and transition temperature are the same as those defined in Figs. 1 and 3 (see text). Compared with the $(R^{3+}_{0.5}A^{2+}_{0.5})MnO_3$, $RBaMn_2O_6$ has two remarkable features: (1) relatively high T_{CO} and (2) the presence of structural transition above T_{CO} in $RBaMn_2O_6$ with R^{3+} of small ionic radii (the existence of the second paramagnetic metal PM' phase).

The results are summarized in Fig. 4 in a phase diagram. Here we express the phase diagram as a function of the ratio of ionic radius, $r_I = r_{R^{3+}}/r_{Ba^{2+}}$,[8] instead of f. In $RBaMn_2O_6$, the MnO_2 sublattice is sandwiched by two types of rock-salt layers, *R*O and BaO, with different lattice sizes, as shown in Fig. 2(b), and therefore the tolerance factor cannot be defined. r_I is a measure of mismatch between *R*O and BaO lattices.

It is very interesting to compare Fig. 4 with Fig. 1. Figure 4 is similar to Fig. 1, generally. There exist characteristic phases such as the FM phase and the CE-type COI(CE) phase in both phase diagrams. In Fig. 4, the FM phase is stable around $R = La$ and the COI(CE) phase becomes dominant for $Sm \sim Ho$ and Y. The ionic size of Ba^{2+} (1.61 Å)[8] is much larger than those of Sr^{2+} (1.44 Å) and all of R^{3+} ($\leq$1.36 Å). In $RBaMn_2O_6$, the MnO_2 layer feels opposite strain forces from the adjacent *R*O and BaO layers; as a result, the MnO_6 octahedron itself is distorted in a peculiar manner that the oxygen atoms of the MnO_2 square lattice are strongly bound by R^{3+} resulting in buckling of Mn and oxygen atoms in the MnO_2 square plane,[5] in contrast to the rigid MnO_6 octahedron in $(R^{3+}_{0.5}A^{2+}_{0.5})MnO_3$. Among the combination of R^{3+}/Ba^{2+}, the mismatch between *R*O and BaO lattices is the smallest in La^{3+}/Ba^2, the second smallest in Pr^{3+}/Ba^{2+} and the third smallest in Nd^{3+}/Ba^{2+}. It is expected that the FM appears in these compounds with a relatively small lattice mismatch and no tilt of MnO_6 octahedra. In these compounds, T_C is about 300 K, and is slightly dependent on r_I. This suggests that the ferromagnetic interaction or DE interaction is not highly influenced by the lattice distortion in $RBaMn_2O_6$, which is supported by the finding that the positive Weiss temperature $\theta = 286$ K is observed even in the PM region ($T > T_t$) of $YBaMn_2O_6$ with the largest lattice distortion.[3] On the other hand, the

COI(CE) phase appears in $R\mathrm{BaMn_2O_6}$ ($R = \mathrm{Sm} \sim \mathrm{Ho}$ and Y) with a larger lattice mismatch and the tilt of $\mathrm{MnO_6}$ octahedra. The observed T_{CO} ($\geq$340 K) is much higher than that (<300 K) for $(R^{3+}_{0.5}A^{2+}_{0.5})\mathrm{MnO_3}$, and it increases with decreasing r_I. This suggests that the lattice distortion in $R\mathrm{BaMn_2O_6}$ efficiently enhances the CO interaction in contrast to ferromagnetic interaction; as a result, the CO interaction exceeds the ferromagnetic DE interaction. This could be one of the reasons for the absence of FM to antiferromagnetic CE-type COI(AFI(CE)) transition in $R\mathrm{BaMn_2O_6}$.

There are remarkable features in the phase diagram of $R\mathrm{BaMn_2O_6}$: (1) the high T_{CO} and (2) the presence of a structural transition at T_t above T_{CO}. It is easy to understand this relatively high T_{CO} in $R\mathrm{BaMn_2O_6}$, because the absence of *A*-site randomness and the layer-type metal-order are favorable for the CO of $\mathrm{Mn^{3+}/Mn^{4+}}$. As mentioned above, the increase of the mismatch between *R*O and BaO lattices also makes the CO stable. The structural transition at T_t is a characteristic of compounds with R^{3+} of small ionic radii. The large mismatch between *R*O and BaO lattices introduces a strong frustration to the $\mathrm{MnO_2}$ sublattice; as a result, the $\mathrm{MnO_6}$ octahedron itself is heavily distorted leading to a complex structural deformation (triclinic or monoclinic).[5] Such deformation must give a new perturbation to the competition of multi-degrees of freedom among charge, orbital, spin and lattice. The paramagnetic metal phase (PM') with an antiferromagnetic correlation and a pseudo-tetragonal structure (isotropic *a*–*b* plane) between T_t and T_{CO} inspire us to study the possibility of orbital ordering, presumably $d_{x^2-y^2}$-type, at T_t. The freezing of the orbital, charge and spin degrees of freedom at independent temperatures may become possible in structures with low symmetry such as asymmetric distortion of the $\mathrm{MnO_6}$ octahedron.

In summary, the structures and electromagnetic properties of new metal-ordered perovskite manganites $R\mathrm{BaMn_2O_6}$ (R = Y and rare earth elements) have been investigated. $R\mathrm{BaMn_2O_6}$ can be classified into three groups based on the obtained structural and electromagnetic properties. The first group (R = Tb, Dy and Ho) shows three successive phase transitions, namely, structural, CO (MI) and AF transitions. The second group (R = Sm, Eu and Gd) exhibits the CO (MI) transition, followed by the AF transition. The third group (R = La, Pr and Nd) exhibits the FM transition, followed by the *A*-type AFM transition in $\mathrm{PrBaMn_2O_6}$ or $\mathrm{NdBaMn_2O_6}$. Compared with metal-disordered $(R^{3+}_{0.5}A^{2+}_{0.5})\mathrm{MnO_3}$, $R\mathrm{BaMn_2O_6}$ has two remarkable features: (1) the relatively high T_{CO} and (2) the presence of structural transition without any charge and magnetic order above T_{CO} in the first group. These are closely related to the metal-ordered structure with the distorted $\mathrm{MnO_6}$ octahedra.

The authors thank T. Yamauchi, M. Isobe, T. Matsushita, Z. Hiroi and H. Fukuyama for valuable discussion. This work is partly supported by Grants-in-Aid for Scientific Research (Nos. 407 and 758) and for Creative Scientific Research (No. 13NP0201) from the Ministry of Education, Culture, Sports, Science, and Technology.

1) See reviews, C. N. R. Rao and B. Raveau: *Colossal Magnetoresistance, Charge Ordering and Related Properties of Manganese Oxides* (World Scientific, Singapore, 1998).
2) S. Mori, C. H. Chen and S.-W. Cheong: Phys. Rev. Lett. **81** (1998) 3972.
3) T. Nakajima, H. Kageyama and Y. Ueda: J. Phys. Chem. Solids **63** (2002) 913.
4) H. Kageyama *et al.*: cond-mat/0208518.
5) T. Nakajima *et al.*: submitted to J. Solid State Chem.
6) F. Millange, V. Caignaert, B. Domengès and B. Raveau: Chem. Mater. **10** (1998) 1974.
7) H. Kawano, R. Kajimoto, H. Yoshizawa, Y. Tomioka, H. Kuwahara and Y. Tokura: Phys. Rev. Lett. **78** (1997) 4253.
8) R. D. Shannon: Acta Crystallogr. A **32** (1976) 751.